Available online at www.sciencedirect.com

SciVerse ScienceDirect

journal homepage: www.elsevier.com/locate/he

# Stability of Ni and Rh–Ni catalysts derived from hydrotalcite-like precursors for the partial oxidation of methane

*Deborah V. Cesar* [a,b], *Maria A.S. Baldanza* [a], *Cristiane A. Henriques* [a,b], *Francisco Pompeo* [c], *Gerardo Santori* [c], *John Múnera* [d], *Eduardo Lombardo* [d], *Martin Schmal* [a], *Laura Cornaglia* [d], *Nora Nichio* [c,*]

[a] *UFRJ/COPPE/NUCAT Núcleo de Catálise -Programa de Engenharia Química - Universidade Federal do Rio de Janeiro - Caixa Postal 68502 Rio de Janeiro 21945-970, RJ, Brazil*

[b] *UERJ/IQ/PPGEQ – Programa de Pós-graduação em Engenharia Química – Instituto de Química – Universidade do Estado do Rio de Janeiro, Rio de Janeiro, RJ, Brazil*

[c] *CINDECA, y Facultad de Ingeniería, UNLP-CONICET, 47 No. 257, 1900 La Plata, Argentina*

[d] *INCAPE (FIQ, UNL-CONICET), Santiago del Estero 2829, 3000 Santa Fe, Argentina*

ARTICLE INFO

*Article history:*
Received 17 December 2012
Received in revised form
12 February 2013
Accepted 13 February 2013
Available online 22 March 2013

*Keywords:*
Ni
Rh
Hydrotalcites
Hydrogen
Methane
Partial oxidation

ABSTRACT

In this work, NiMgAl and RhNiMgAl catalysts prepared from HTLCs precursors were investigated for the Partial Oxidation of Methane (POM) at 550 and 750 °C. Samples have been characterized by XRD, TPR, $H_2$ chemisorption, TPSR analyses, XPS, field emission scanning electron microscopy and Raman spectroscopy. NiMgAl catalysts with high Ni content (40 and 16 wt%) showed high stability and high methane conversion for POM. On the other hand those with lower Ni content (NiHT15 and NiHT25, with 6 and 4 wt%) exhibited low catalytic activity with low $H_2$/CO ratio (<2) and fast deactivation. In RhNiHT25 (0.6 wt. % Rh), the Ni reducibility was improved, increasing the methane conversion and hydrogen selectivity. In addition, the noticeable increase in stability was related to the absence of carbon deposition after 30 h on stream at 550 °C. These results show that RhNiHT25 is promising for application in membrane reactors to produce high purity hydrogen.



## 1. Introduction

In the last few years, there has been a significant progress in the study of hydrogen generation from alternative sources other than fossil fuels. However, natural gas has proven to be increasingly competitive in relation to various other fuels, either in the industrial sector or in power generation. According to the International Energy Agency (IEA) [1], the demand for natural gas in energy production will keep expanding until 2020. Methane is the main component in natural gas and due to its economic feasibility it has become the main source of synthesis gas and hydrogen produced from steam reforming. Partial oxidation (POM) is a promising substitute for the steam reforming process since it is economical, shows high conversion and selectivity to hydrogen besides the production of $H_2$ and CO in a ratio of 2, which is suitable for the Fischer Tropsch synthesis [2]. Moreover, the low endothermicity and the short contact time of the process are interesting features if small or medium-sized plants are projected [3]. On the other hand, due to the high temperatures

* *Corresponding author.*
E-mail address: nnichio@quimica.unlp.edu.ar (N. Nichio).

0360-3199/$ – see front matter 
http://dx.doi.org/10.1016/j.ijhydene.2013.02.064

and space velocities, the development of new active and stable catalysts for POM is an issue of interest. Among the different catalysts that have been analyzed, those based on nickel are the most widely studied ones for this reaction and their main advantage is the low cost. However, these catalysts are susceptible to carbon deposition and the active Ni metallic particles can be oxidized even at low temperatures of reaction. This justifies increasing efforts in the study of catalyst formulation in order to obtain stable systems based on Ni. The preparation method and the synthesis parameters are important features since they influence the interactions between the metal and the support playing an important role on the catalytic performance including the prevention of carbon deposition and sintering [4–7].

Thermally treated hydrotalcite-like compounds (HTLCs) lead to mixed oxides with high surface area, thermal stability, basic properties and highly homogeneous dispersion of the elements into the oxide matrix. Many catalytic applications have arisen since the 1990s and are based on basic and/or redox properties, which are associated with stable metallic particles [8–10]. The use of Ni based or noble metal mixed oxides derived from HTLCs as active catalysts for $H_2$ production has been extensively studied, not only for the partial oxidation of methane but also for steam reforming [11], dry reforming [12] and autothermal reforming of methane [13] at reaction temperatures higher than 650 °C [14–17]. However, only a few papers have reported the activity and stability of these materials at low temperatures ($T \sim 550$ °C), which may allow their application on membrane reactors. In the literature, Rh has been studied as a good promoter that increases the activity of the Ni catalysts and decreases the carbon deposition [6,7]. However, several authors have claimed that Rh–NiMgAl catalysts present higher rates of carbon deposition, in the dry reforming and POM reactions, suggesting that carbon deposition occurred because Rh favors $CH_4$ decomposition [18].

In this work, Ni–Mg–Al catalysts prepared from HTLCs precursors were investigated for the POM reaction at 550 and 750 °C. Since carbon deposition is a key negative factor for use in Pd based membrane reactors, we have also studied the effect of Ni content and Rh incorporation on the catalytic behavior. Special attention was paid to the stability of these formulations in connection with carbon deposition.

## 2. Experimental

### 2.1. Catalyst preparation

Hydrotalcite samples were prepared by coprecipitating an aqueous solution of nickel, magnesium and aluminum cations (solution A) with a highly basic carbonate solution (solution B) at room temperature. Solution A, containing $Ni(NO_3)_2 \cdot 6H_2O$, $Mg(NO_3)_2 \cdot 6H_2O$ and $Al(NO_3)_3 \cdot 9H_2O$ dissolved in distilled water was 1.5 mol $L^{-1}$ in (Al + Mg + Ni) with an Al/(Al + Mg + Ni) molar ratio equal to 0.25 and a Ni/Mg molar ratio of 1/1, 1/5, 1/15, and 1/25. Solution B was prepared by dissolving appropriate amounts of $Na_2CO_3$ and NaOH in distilled water in order to obtain a $[CO_3^{2-}]$ equal to 1.0 mol $L^{-1}$ and a pH equal to 13 during the ageing of the gel. In the synthesis procedure, solution A was slowly added (60 mL $h^{-1}$) under vigorous stirring to a B solution placed in a 150 mL PTFE reactor. The gel formed was aged under constant pH (13) for 18 h at 60 °C. The solid obtained was then filtered and washed with distilled water (90 °C) up to pH = 7.

The Ni–Mg–Al-hydrotalcites obtained were dried in air at 80 °C during 12 h and were denoted as "NiHTX-nc", where X is the Mg/Ni molar ratio and nc means not calcined. A Mg,Al-hydrotalcite (HT-nc) was prepared by the same methodology and used as reference in the physicochemical characterization.

The Ni–Mg–Al mixed oxides were obtained through calcination of the HTLCs precursors under dry air, from room temperature to 500 °C, using a heating rate of 5 °C $min^{-1}$. The calcined samples were denoted as NiHTX, X being defined as above.

The Rh catalysts were prepared by the conventional wet impregnation of $RhCl_3 \cdot 3H_2O$ onto calcined HT and NiHT25 mixed oxides. The impregnated solids were then heated at 80 °C to evaporate the water, and dried at 110 °C overnight. The catalysts were calcined for 6 h at 500 °C in flowing air. The bimetallic solid presented a molar ratio of Ni/Rh = 10 with 0.6 wt. % of Rh in all samples.

### 2.2. Physicochemical characterization

The chemical composition of the samples was determined by X-ray fluorescence analysis (XRF), using a Rigaku spectrometer, model Rix 3100, controlled by software Rix 3100, with an X-ray tube of Rh anode. The textural characteristics, specific surface area and pore volume (BJH method) were determined by $N_2$ physisorption at −196 °C in a Micromeritics ASAP 2000. Prior to the analyses, the samples were outgassed for 20 h at 200 °C (as-synthesized) or at 450 °C (mixed oxides).

X-ray diffraction (XRD) was performed in a Miniflex/Rigaku diffractometer, using CuK$\alpha$ radiation, with a voltage of 30 kV and a current of 15 mA. The diffractograms of calcined and reduced samples were registered in Bragg angles ($2\theta$) from 2° to 90° with steps of 0.05° at 1 s/step. The evaluation of the metallic phases was done after the reduction of the samples *ex-situ* at 900 °C with pure $H_2$ (30 mL $min^{-1}$; 10 °C $min^{-1}$) for 60 min. Afterwards, the sample was cooled down under Ar (30 mL $min^{-1}$) until room temperature was achieved. Then, the passivation process was carried out flowing a stream of 5% $O_2$/He (30 mL $min^{-1}$) for 30 min through the sample kept at −80 °C, followed by a treatment under Ar (30 mL $min^{-1}$) for 15 min at this temperature and for 30 min at room temperature. The Rietveld method was used to quantify the NiO and Ni phases formed [19].

The temperature-programmed reduction tests (TPR) were performed in a conventional dynamic equipment, with a $H_2$/$N_2$ ratio in the 1/9 feed and heating at 10 °C $min^{-1}$ from room temperature to 900 °C.

The $H_2$ chemisorption was performed in a dynamic equipment with a TCD detector. The calcined samples were reduced under hydrogen at 700 °C for 1 h, and then they were cooled down under hydrogen flow (50 mL $min^{-1}$) to 400 °C and then treated under Ar (50 mL $min^{-1}$) during 2 h at 400 °C. Finally, the samples were cooled down to room temperature under Ar (50 mL $min^{-1}$) and pulses of pure hydrogen were applied until saturation was achieved. Nickel dispersion was

determined according to the quantity of hydrogen uptake, assuming an adsorption stoichiometry of H/Ni = 1.

Temperature-Programmed Surface reaction analyses (TPSR) were performed on a multipurpose unit equipped with a fixed-bed reactor operating at atmospheric pressure. The samples were reduced from room temperature up to 550 °C for 1 h, under pure $H_2$ flow (30 mL $min^{-1}$) and then cooled down to 300 °C or kept at 550 °C under flow of He in order to evaluate the temperature influence. After stabilizing the temperature, the reaction mixture was fed into the reactor with a composition of $N_2/CH_4/O_2 = 7/2/1$ (space velocity of $2 \times 10^6$ $cm^3$ $h^{-1}$ $g^{-1}$). The temperature ranges employed were 300 or 550 °C to 900 °C. Using a quadrupole mass spectrometer (QMS 422, Balzers, PRISMA), the products were monitored by their characteristic mass fragmentation patterns *m/e* signals: 2 ($H_2$), 15 ($CH_4$), 18 ($H_2O$), 28 (CO), 32 ($O_2$) and 44 ($CO_2$).

The X-ray photoelectron spectroscopy (XPS) analyses were performed in a Multi-Technique UniSpecs equipment with a dual X-ray Mg/Al source and a hemispheric analyzer PHOIBOS 150. The spectra were obtained with a pass energy of 30 eV and the Mg-K$\alpha$X-ray source was operated at 200 W and 12 kV. The working pressure in the analyzing chamber was less than $6 \times 10^{-7}$ Pa.

Prior to the measurements, the samples were reduced in flowing hydrogen in a fixed-bed reactor at 750 °C. After being exposed to air, the samples were treated in a $H_2$/Ar flow at 400 °C in the reaction chamber attached to the instrument.

To calculate the surface concentrations, the spectra of Ni 2*p*, Mg 2*p*, Rh 3*d* and Al 2*s* were analyzed. The spectrum of Al 2*p* was not considered due to the overlapping with the Ni 3*p* peak and the Auger Mg KLL peak. The peak areas were determined by integration employing a Shirley-type background. Peaks were considered to be a mixture of Gaussian and Lorentzian functions in a 70/30 ratio. For the quantification of the elements, sensitivity factors provided by the manufacturer were used.

The post-reaction samples were analyzed in a field emission scanning electron microscope (FEG SEM) model Quanta 400 da FEI (30 kV). The analyses were performed under high-vacuum, with voltages from 20 to 30 kV with no metallic coating.

The carbon deposits were studied using Laser Raman Spectroscopy (LRS) in a LabRAM HR UV 800 (Horiba/Jobin-Yvon) instrument, laser He–Ne ($\lambda = 632$ nm), CCD detector and an OLYMPUS microscope, model BX41. The measurements of the samples, diluted in KBr, were taken with a 100× magnification and the scattered light was collected through a confocal hole of 100 μm.

### 2.3. Catalytic tests

The catalytic activity tests were performed in a continuous-flow reactor operating at atmospheric pressure. Operating conditions with respect to total feed flow rate and average catalyst particle size were defined so as to eliminate intra-phase and interphase transport resistances. When highly exothermic reactions, as in this case, are carried out in experimental reactors it is necessary to take into account two very important facts: temperature gradient between gas phase and solid phase and the hot spots that can develop within the catalyst bed. Both factors have been deeply analyzed. With respect to temperature gradient between both phases, and considering that the controlling mechanism is in the gas solid film following the procedure of Froment and Bischoff the maximum temperature gradient estimated in the film is approximately 10 K, considering methane combustion as the only reaction (heat of combustion of methane ~190 kcal/mol) [20]. Several factors affecting the presence and magnitude of hot spots were investigated: contact time, solid dilution and gas dilution. The magnitude of the hot spots is quantified by the temperature difference registered by two thermocouples, one within the catalysts bed (Ti) and one prior to the catalyst bed (Tu). Under the experimental condition employed, the axial temperature gradient in the reactor was 5 °C (Ti–Tu). Taking into account the preceding results, the following experimental conditions were selected: atmospheric pressure, temperature range between 550 and 750 °C, a space velocity of $6.4 \times 10^5$ $cm^3$ $h^{-1}$ $g^{-1}$, a feed mixture POM: $N_2/CH_4/O_2 = 7/2/1$, catalyst/inert ratio: 1/10.

The previously calcined samples were reduced in flowing $H_2$ flow (30 $cm^3$ $min^{-1}$) increasing the temperature from 25 °C to 750 °C at 10 °C $min^{-1}$ and then keeping the system at 750 °C for 1 h. The stability test was performed at constant temperature. The stability was evaluated in terms of the $\mathbf{a_{CH4}}$ decay ratio, which represents the ratio between the $CH_4$ consumption rate at time *t* (hours) and the initial rate.

## 3. Results and discussion

### 3.1. Physicochemical characterization

#### 3.1.1. Ni–Mg–Al catalyst

The chemical composition and general formula of dehydrated samples prepared with different Mg/Ni molar ratios (1/1, 5/1, 15/1 and 25/1) are presented in Table 1. They are similar to those of the synthesis gel, indicating an approximately

**Table 1 – Chemical composition and general formula (dehydrated form) of the as-synthesized HTLCs.**

| Sample | Mg/Ni | Al/(Al + Mg + Ni) | *a* (Å)[a] | *c* (Å)[a] | Formula |
|---|---|---|---|---|---|
| NiHT1-nc | 1.0 | 0.22 | n.d. | n.d. | $Ni_{3.10}Mg_{3.12}Al_{1.78}(OH)_{16}(CO_3)_{0.89}$ |
| NiHT5-nc | 5.0 | 0.24 | 3.050 | 23.113 | $Ni_{1.,01}Mg_{5.07}Al_{1.92}(OH)_{16}(CO_3)_{0.96}$ |
| NiHT15-nc | 15 | 0.24 | 3.060 | 23.317 | $Ni_{0.38}Mg_{5.70}Al_{1.92}(OH)_{16}(CO_3)_{0.96}$ |
| NiHT25-nc | 24 | 0.24 | 3.060 | 23.202 | $Ni_{0.24}Mg_{5.84}Al_{1.92}(OH)_{16}(CO_3)_{0.96}$ |

n.d., Not determined.
a Lattice parameters calculated from XRD.

complete incorporation of the cations in the HTLC structure. The lattice parameters (*a* and *c*), which characterize the hydrotalcite-like structure are also shown.

Regarding the lattice parameters *a* and *c*, it is well known that for a classical rhombohedral 3R stacking symmetry of hydrotalcites, the lattice parameter *a* is associated with the cation–cation distance in the hydroxide layer and *c* is equal to 3*c*′, where *c*′ is the thickness between a brucite-like sheet and one interlayer [21]. These parameters were determined from the crystallographic planes (003), (006), (110) and (113) and it can be seen that they agree with those reported in the literature for this type of material [22,23].

Textural properties of the as-synthesized samples (HT-nc and NiHTX-nc) were not significantly influenced by the nickel presence or by the differences in the amount of this metal. BET surface areas are relatively low and varied in the range 60–80 $m^2\ g^{-1}$, whereas pore volumes (BJH) varied between 0.38 and 0.50 $cm^3\ g^{-1}$. Upon calcination at 500 °C, both specific surface areas and pore volumes increased, mainly due to the formation of mesopores with diameter in the 20–50 Å range. The formation of these mesopores can be associated with the elimination of carbonate anions, through the release of $CO_2$, beginning at about 270 °C and leading to partial destruction of the layered structure (as observed by XRD) giving rise to holes, the so-called "craters" [24]. This "cratering" of the samples could be responsible for the increase observed in the surface area and pore volume. With the increase of Ni content, a reduction of both the BET surface area (290–240 $m^2\ g^{-1}$) and the pore volume (0.51–0.46 $cm^3\ g^{-1}$) was observed.

There is a divergence in the literature with respect to the calcination temperature of the HTLCs which would lead to the segregation of a spinel-phase of Ni and Al [23,25]. Our results agree with those that propose calcination temperatures higher than 750 °C for this spinel formation.

X-ray diffraction results of calcined samples are shown in Fig. 1. As can be seen in Fig. 1a, the diffractogram of sample HT (without Ni) presents the characteristic peaks of the periclase phase (MgO) at $2\theta = 36, 43, 62, 74$ and 79° (JCPDS 75-1525) with a contribution of the spinel-phase ($MgAl_2O_4$) at $2\theta = 44$, 74 and 78° (JCPDS 21-1152). With the addition of Ni, a broadening of the peaks can be observed, which would indicate the incorporation of Ni in the Mg and Mg–Al oxide structure. The diffraction profiles of the catalysts with lower Ni content (NiHT25 and NiHT15) are very similar to those of HT and a slight decrease of the peak intensity at $2\theta \sim 74°$ can be observed. There is no evidence of the NiO phase, and Ni might form a mixed phase with MgO and/or $MgAl_2O_4$. When the Ni content increases, it can be observed that the intensity of the peaks at $2\theta \sim 37$ and 75° increases, indicating the formation of a NiO phase (JCPDS 47-1049) [26,27] in the NiTH1 sample. It is important to remark that it is difficult to distinguish between the spinel structures ($Mg_xAl_{2-x}O_4$ or $Ni_xAl_{2-x}O_4$) and the periclase (MgO or $Ni_xMg_{1-x}O$) because the characteristic diffraction peaks overlap.

The analysis of the diffractograms of the catalysts reduced *ex-situ* at 750 °C during 1 h in pure $H_2$ (Fig. 2), followed by the passivation process, indicates the segregation of the metallic Ni at $2\theta = 44.6$ and 51.8° (JCPDS 04-0850) and the characteristic peaks of MgO and $MgAl_2O_4$ phases for the NiHT1 and NiHT5 samples [28].

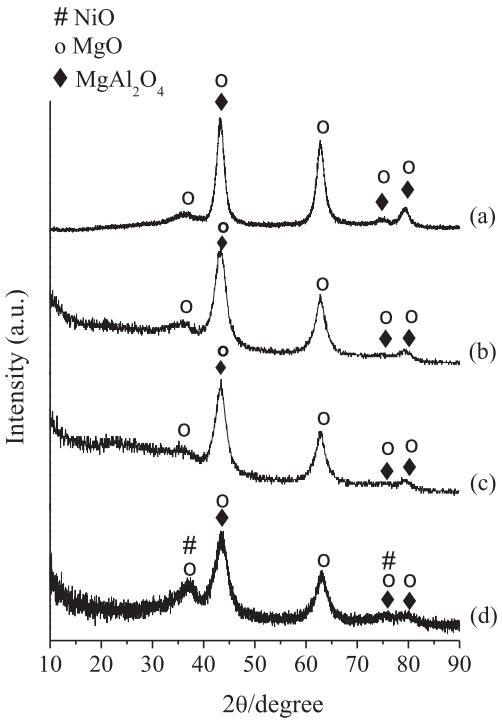


**Fig. 1 – X-ray diffractograms of the calcined samples at 500 °C. (a) HT; (b) NiHT25; (c) NiHT15; (d) NiHT1.**

Table 2 shows the chemical composition of the samples reduced *ex-situ* at 750 °C obtained through the Rietveld refinement of XRD data. The XRF results are also shown and were used to compare with the relative quantity obtained from refinement. In the samples studied, the application of the Rietveld method enabled the relative quantification of the phases present and they are consistent with the values obtained by XRF for the NiHT1 and NiHT5 samples. The catalysts with low nickel content, NiHT15 and NiHT25, show very low percentage of $Ni^0$ detected by XRD. This could be not only due to the low content of nickel, but also to the presence of small metallic particles that goes undetected by XRD [19,29,30]. In the $2\theta = 31–39°$ region, the fitting of the experimental and calculated patterns was even more difficult probably due to the fact that some planes could correspond to phases with a certain degree of disorder. In particular, we are referring to plane (111) that corresponds to $2\theta = 38.1°$ of the NiO phase (Bunsenite) and plane (220) at $2\theta = 34.8°$ of $MgAl_2O_4$. However, this difficulty does not interfere in the evaluation of the quantities of segregated Ni.

Table 2 also summarizes the extent of reduction of the NiHTX samples under study; showing low Ni reducibilities. The TPR profiles (not shown) exhibited high temperatures of reduction (≥800 °C) for all samples, which would correspond to a strong interaction between nickel species and the mixed oxide matrix. The NiHT1 sample also showed small hydrogen consumption at lower temperature (500 °C). This consumption could be associated with the presence of NiO detected by XRD. This is in agreement with the highest Ni content in this sample. As the nickel content decreased, the maximum temperature of $H_2$ consumption shifted to higher temperatures (>950 °C). For NiHT25, the highest temperature of

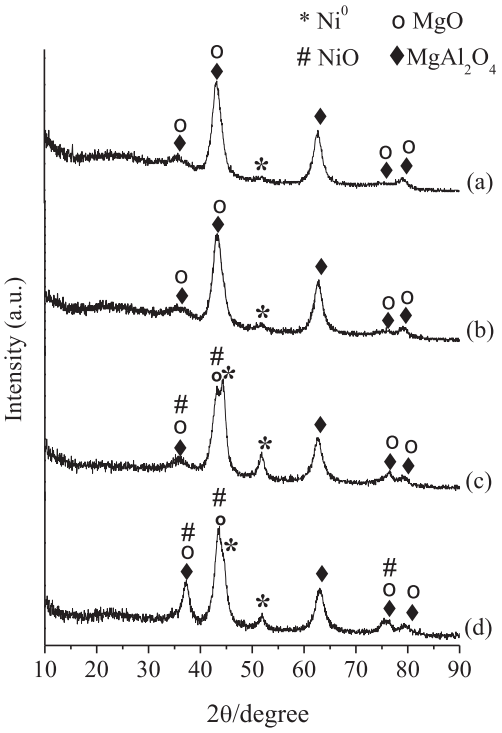


**Fig. 2 – X-ray diffractograms of the samples reduced *ex-situ* at 750 °C during 1 h in pure $H_2$ followed by passivation process. (a) NiHT25; (b) NiHT15; (c) NiHT5; (d) NiHT1.**

consumption could not be determined due to the fact that the maximum temperature reached by the instrument is 1000 °C. Thus, these results suggest that the lower the Ni content the lower is its reducibility, and are consistent with the hydrogen chemisorption data (Table 2). According to Basile et al. [15,16], the reducibility of Ni depends on the Ni/Mg ratio in the mixed phase (Ni,Mg,O) formed during calcination and on the Mg/Al ratio of the HT-like precursor. Our catalysts have an Mg/Al ratio that varies from 1.7 to 3.0 and according to Basile and coworkers the catalysts with an Mg/Al ratio ~2 show partial reduction of $Ni^{2+}$. Therefore, the small amount of $H_2$ chemisorbed is due to the low extent of nickel reduction, and not to a drop in the metallic dispersion. Thus, the TPR results are in agreement with the $Ni^0$ content calculated by the Rietveld method.

### 3.1.2. *Rh–Ni–Mg–Al catalyst*

The characterization results for Rh-containing catalysts and NiHT25 samples are shown in Table 3.

Reducibility results (from TPR analyses) of the RhNiHT25 and RhHT samples are also presented, including the maximum temperature for the main peak of hydrogen consumption and the extent of reduction (% of reduction). The RhNiHT25 catalyst showed a marked increase in the Ni reduction compared to the NiHT25 catalyst and a decrease of approximately 200 °C in the maximum temperature of the reduction peak. In RhHT, $Rh_2O_3$ was completely reduced below ~400 °C.

The diffraction profile of the RhNiHT25 catalyst (not shown) was similar to that of the NiHT25 catalyst; then, it was not possible to determine any structural changes after Rh impregnation. In addition, no reflections peaks from crystalline Rh oxides were detected in the calcined solid although XPS measurements show differences in the surface oxidation state for Rh. The XPS results of the reduced samples are also shown in Table 3, where it can be observed that the surface intensity ratios exhibit differences with respect to the volumetric ones determined by XRF. For all catalysts, the surface Ni/Mg ratios are significantly smaller than that of the volume, while the Al/Mg and Rh/Mg ratios present slight variations.

The Rh $3d_{5/2}$ spectrum for the reduced RhHT catalyst shows only one peak assigned to $Rh^0$ at 306.7 eV (Fig. 3). On the other hand, the spectrum of the reduced RhNiHT25 solid presents two signals, one corresponding to $Rh^0$ (306.7 eV) and the other belonging to $Rh^{n+}$ (309.4 eV).

Values in the 307.6–309.6 eV range for $Rh^+$ compounds were reported by Nefedov et al. [31]. However, other authors [32] reported BEs for $Rh^{2+}$ compounds within a similar range (308.4–309.3 eV). The $Rh^{3+}$ presents a binding energy of 309.7 eV and for pure Rh metal foil the Rh $3d_{5/2}$ peak appears at 307.0 eV, with 1.6 eV FWHM [33].

**Table 2 – Chemical composition results and other features of the samples.**

| Sample | XRF (%wt) | | | Mg/Al | Mg/Ni | % Phases[a] reduced 750 °C | $d_p$[b] (nm) | TPR | | %D[c] |
|---|---|---|---|---|---|---|---|---|---|---|
| | %Ni | %Mg | %Al | | | | | $T_{max}$ (°C) | %Red | |
| NiHT1 | 40 | 17 | 11 | 1.7 | 1.0 | 40% $Ni^0$<br>5.0% NiO<br>55% ($MgAl_2O_4$ + MgO) | 6 | 890 | 60 | 9 |
| NiHT5 | 16 | 32 | 14 | 2.6 | 5.0 | 12% $Ni^0$<br>2.0% NiO<br>86% ($MgAl_2O_4$ + MgO) | 7 | 993 | 31 | 5 |
| NiHT15 | 6 | 39 | 14 | 3.0 | 15 | 1.0% $Ni^0$<br>3.0% NiO<br>96% ($MgAl_2O_4$ +MgO) | n.d. | 1000 | 16 | 1.5 |
| NiHT25 | 4 | 40 | 15 | 3.0 | 24 | 0.2% $Ni^0$<br>99.8% ($MgAl_2O_4$ +MgO) | n.d. | n.d. | 12 | n.d. |

a wt.% of phases calculated by the Rietveld method.
b $d_{crist}$, calculated from the diffraction peak at $2\theta = 51.8°$.
c Dispersion calculated from hydrogen chemisorption data.

**Table 3 – TPR and XPS results of the samples reduced at 750 °C.**

| Sample | $T_{max}$ | Reduction (%) | XRF | | | XPS | | |
|---|---|---|---|---|---|---|---|---|
| | | | Al/Mg | Ni/Mg | Rh/Mg | Al/Mg | Ni/Mg | Rh/Mg |
| RhNiHT25 | 834 | 100 | 0.33 | 0.040 | 0.0035 | 0.36 | 0.021[a] | 0.003 |
| Calcined | | | 0.33 | 0.040 | 0.0035 | 0.42 | 0.023 | 0.006 |
| RhHT | 330 | 99 | 0.33 | – | 0.0035 | 0.41 | – | 0.003 |
| Calcined | | | 0.33 | – | 0.0035 | 0.37 | – | 0.004 |
| NiHT25 | >1000 | 12 | 0.35 | 0.041 | – | 0.36 | 0.025[a] | – |

a Samples reduced at 750 °C were exposed to $H_2$/Ar flow at 400 °C in the reaction chamber attached to the spectrometer.

The binding energy (BE) of Ni $2p_{3/2}$ was the same in both samples. The value of 855.2 eV could be assigned to species of Ni (II) strongly interacting with the aluminum based support. Note that in both samples the nominal Ni/Mg ratio is equal to 0.04. In the case of hydrotalcites with high concentrations of Ni (Ni/Mg in the volume equal to 3.7), Romero et al. [34] found that Ni at the surface can be partially reduced to $Ni^0$ (BE = 852.3 eV) at temperatures of 720 °C. Our XPS results suggest that in the bimetallic Ni–Rh catalyst, surface RhOx species are more difficult to reduce than the Rh species present in the monometallic one. In the same way, Ferrandon et al. [35], through XAFS analyses, found that Ni–Rh/La–$Al_2O_3$ catalysts contain rhodium oxide species that are harder to reduce than those in monometallic Rh. In addition, they reported discrepancy between XAFS and TPR results, because TPR could not differentiate between the reduction of highly oxidized nickel species and that of the "hard-to-reduce" oxidized rhodium species due to the fact that both species are reduced in the same temperature range. In those catalysts, the reduction of the rhodium species occurred at the same temperature as the reduction of $NiAl_2O_4$, suggesting that rhodium might be incorporated into the spinel lattice. A similar behavior was observed in our RhNiHT25 solid, where we detected hard-to-reduce rhodium species through XPS measurements (Fig. 3).

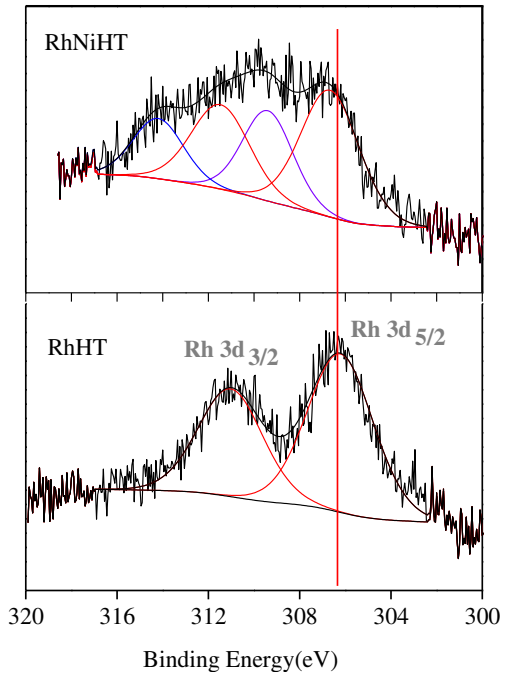


**Fig. 3 – XPS Rh 3*d* spectra for RhNIHT25 and RhHT catalysts after reduction at 750 °C followed by $H_2$/Ar treatment at 400 °C in the reaction chamber attached to the spectrometer.**

### 3.2. *Catalytic activity in POM reaction*

The TPSR tests were done with reduced samples at high spatial velocity ($2.0 \times 10^6$ $cm^3$ $h^{-1}$ $g^{-1}$). Fig. 4a and b shows the results for NiHT1 when the reaction mixture was fed at 300 °C. Together with the disappearance of $CH_4$ and $O_2$, it is also shown that around 400 °C the production of $CO_2$ and $H_2O$ increases due to the total oxidation of $CH_4$. At 500 °C, $H_2$ appears simultaneously with CO, $CO_2$ and $H_2O$ (Fig. 4b). This would indicate the coexistence of two reaction mechanisms: (i) a one-step mechanism, through direct partial oxidation in which CO is the primary product (reaction (1)); and (ii) a two-step mechanism, in which the total oxidation of $CH_4$ to produce $CO_2$ and $H_2O$ (reaction (2)) takes place first and, afterwards, there occurs the $CH_4$ reforming with $CO_2$ and/or $H_2O$ ((3) and (4)).

$$CH_4 + 1/2O_2 = CO + 2H_2 \quad (1)$$

$$CH_4 + 2O_2 = CO_2 + 2H_2O \quad (2)$$

$$CH_4 + CO_2 = 2CO + 2H_2 \quad (3)$$

$$CH_4 + H_2O = CO + 3H_2 \quad (4)$$

$$CO + H_2O = CO_2 + H_2 \quad (5)$$

In addition, the consumption of $CO_2$ and $H_2O$ is well marked at $T \sim 800$ °C. Similar results (not shown) were obtained with catalysts with low Ni content. Shishido et al. [14] observed a similar behavior for the Ni–Mg–Al catalysts with a nickel content of 21.5%.

Furthermore, the un-reduced catalysts were submitted to activation cycles of POM (Fig. 5) in order to evaluate the effect of the reaction atmosphere and temperature (550–950 °C) on $Ni^{2+}$ species. In all tests, it was observed that under 800 °C

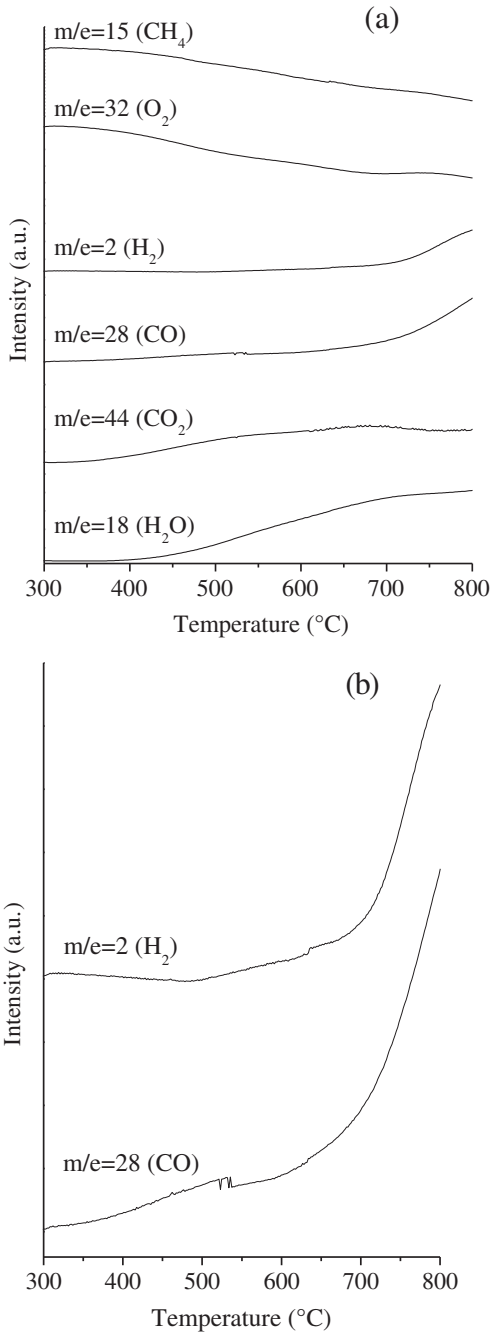


**Fig. 4 – TPSR profiles of NiHT1 reduced at 550 °C, the reaction mixture being fed at 300 °C ($N_2/CH_4/O_2$ = 7/2/1). (a) Characteristic mass fragmentation patterns *m/e* signals: 2 ($H_2$), 15 ($CH_4$), 18 ($H_2O$), 28 (CO), 32 ($O_2$) and 44 ($CO_2$); (b) signal of *m/e* = 2 and 28 with enhanced intensity.**

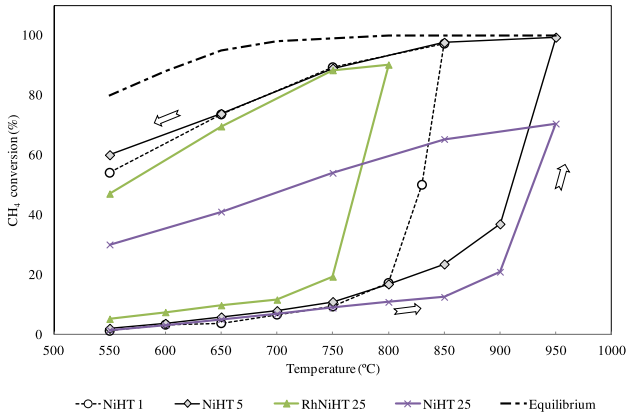


**Fig. 5 – Activation cycles of POM. Methane conversion (%) depending on the temperature – catalysts without previous reduction.**

both the conversion of $CH_4$ (<10%) and the selectivity to CO (not shown) are very low. At the temperatures close to 800 °C for NiHT1 and 900 °C for NiHT5 and NiHT25, a slight increase in the reaction temperature caused an abrupt change in the conversion together with syngas formation. The ignition temperature is dependent on the catalyst composition; the solids with lower Ni content (NiHT5 and NiHT25) presented a higher ignition temperature. For the RhNiHT25 catalyst the ignition temperature is significantly lower in comparison with NiHT25 results. This behavior is related to Ni reducibility since the ignition temperature is lower for the more reducible Ni catalysts (Table 2). The results of the activation cycles follow a similar tendency to the one observed in TPR analyses, where the reduction peak appears at very high temperature (800 °C) and shifts to higher values when the nickel content diminishes [36].

At temperatures higher than the ignition temperature, any change in temperature does not alter the $CH_4$ conversion, which follows the upper part of the curve. When the catalyst sample is previously reduced, the behavior is described by the upper part of the curve. It is important to note that in other systems, such as $Rh_2O_3/Al_2O_3$, the literature shows results in which the abrupt increase of the $CH_4$ conversion and CO selectivity occurs at much lower temperatures ca. 550 °C [37].

The similarity of these results with those of TPSR, together with TPR and XRD data, could indicate that the observed behavior is related to changes in the oxidation state of the Ni active phase. This could be explained by the reaction path where $H_2$ is first generated through the cracking of methane and then this $H_2$ causes the reduction of $Ni^{2+}$ to $Ni^0$. Therefore, the significant difference in the ignition temperature of the reaction is related to the difference in combustion capability and Ni reducibility.

Table 4 shows the results of the catalyst activities at 750 °C and 550 °C. Methane conversion ($X_{CH4}$%), product composition and $H_2$/CO ratio are summarized. The initial activity shows that even the sample with the lowest content of Ni (NiHT25, 4% wt. Ni) is active.

The results at 750 °C show a lower $H_2$/CO ratio for the NiHT15 and NiHT25 solids (1.8 and 1.3 respectively) and for NiHT1 and NiHT5 the ratio was ~2.

When the reaction temperature is decreased to 550 °C the methane conversion decreases and the $H_2$/CO ratio increases. The water gas shift reaction ($CO + H_2O = CO_2 + H_2$) is favored at low temperature; then, it could explain the increase in $H_2$ and $CO_2$ concentration. These results are in agreement with the TPSR data at 550 °C, in which the occurrence of the partial

**Table 4 – Results of the catalytic activity in the POM reaction.**

| Sample | $X_{CH_4}$ [a], % | $X_{O_2}$ [a], % | $H_2$ | CO | $CO_2$, % molar | $H_2$ yield[e], % | $H_2$/CO | $a_{CH_4}$ [b] |
|---|---|---|---|---|---|---|---|---|
| Product composition[a] | | | | | | | | |
| 750 °C | | | | | | | | |
| NiHT1 | 95 | 100 | 68 | 31 | 1 | 98 | 2.1 | 0.98 |
| NiHT5 | 94 | 100 | 68 | 31 | 1 | 96 | 2.2 | 0.98 |
| NiHT15 | 63 | 100 | 61 | 35 | 4 | 68 | 1.8 | 0.98 |
| NiHT25 | 54 | 100 | 58 | 32 | 10 | 49 | 1.3 | 0.70[c] |
| Rh-NiHT25 | 88 | 100 | 66 | 33 | 1 | 87 | 2.0 | 1.0 |
| Rh-HT | 81 | 100 | 66 | 32 | 2 | 83 | 2.0 | 1.0 |
| 550 °C | | | | | | | | |
| NiHT1 | 57 | 100 | 71 | 23 | 6 | 99 | 2.9 | 0.98 |
| NiHT5 | 55 | 100 | 72 | 22 | 6 | 99 | 3.1 | 0.97 |
| NiHT25 | 30 | 97 | 68 | 29 | 3 | 17 | 2.3 | 0[d] |
| Rh-NiHT25 | 47 | 100 | 61 | 20 | 19 | 73 | 2.8 | 1.0 |
| Rh-HT | 53 | 100 | 62 | 23 | 15 | 65 | 2.5 | 1.0 |

a Measured at 2 h on stream. The product composition was calculated on a dry basis.
b After 30 h on stream.
c After 13 h on stream.
d After 5 h on stream.
e $H_2$ yield = ($H_2$ moles/(2 × $CH_4$ reacted)) × 100.

oxidation and a lower consumption of $CO_2$ to reform the methane (3) could be observed.

The stability was evaluated through the decay ratio ($a_{CH_4}$), which is defined as the ratio of the methane conversion at time "t" and the initial conversion of methane. Both high Ni content catalysts, NiHT1 and NiHT5, were stable and exhibited high conversion and hydrogen selectivity. It can be observed that NiHT25 was the least stable catalyst, deactivating after 15 h of reaction (at 750 °C). The post-reaction sample NiHT25 showed a greenish color that suggests the oxidation of the catalyst. It would indicate that at low conversion levels, around 37% at 13 h on stream, the presence of un-reacted oxygen causes nickel oxidation, and consequently, the deactivation of the catalyst.

With respect to the catalytic activity of the bimetallic system, a marked increase in conversion was observed. The RhNiHT25 catalyst showed a methane conversion of 88% and a $H_2$/CO ratio of 2.0 at 750 °C. Furthermore, no deactivation was observed after 30 h on stream. In addition, for the bimetallic catalyst the methane conversion was higher than the conversions obtained for the RhHT solid when the catalytic test was performed at 750 °C. Note that both Rh catalysts (RhNiHT25 and RhHT) were very stable at both reaction temperatures (550 °C and 750 °C) during at least 30 h of reaction. According to the published papers, the excellent coke resistance ability could be assigned to the small amount of noble metals added to Ni catalyst, that might favor the formation of more reactive intermediate carbonaceous species. At the same time, Rh promoted Ni catalyst possess excellent $CO_2$ activation ability and the activated $CO_2$ can supply enough surface oxygen for the gasification of the intermediate carbonaceous species [38].

Concerning the $H_2$/CO ratio, a significant increase was observed with Rh addition (Table 4) in comparison with the value obtained for NiHT25 ($H_2$/CO ratio = 1.3), and a more marked effect could be seen at lower reaction temperature. The effect of Rh addition in the Ni hydrotalcite-like precursor was previously studied by Basile et al. [38,39]. They suggested a possible synergetic effect with higher hydrogen selectivity as compared to the Ni monometallic catalysts. Our results are in agreement with their findings.

### 3.3. Characterization of the carbon deposits

The carbon deposits were studied by laser Raman spectroscopy (LRS), a widely used technique in the analysis of crystalline, nanocrystalline and amorphous carbon. The carbon species show bands in the range of 1000–1700 $cm^{-1}$ and more specifically in approximately 1560 $cm^{-1}$ (G band) and 1360 $cm^{-1}$ (D band) when the excitation is in the visible region. The G band is related to the stretching vibration mode $E_{2g}$ in C=C (C $sp^2$) bond and the D band refers to the $A_{2g}$ mode due to the breathing mode of sixfold ring [40,41]. According to Narksitipan et al. [40], this mode is only active when it occurs in a distorted system. Thus, the width, intensity and position of the bands are modified according to their allotropic form. The band assigned to disordered graphitic form appears at 1340 $cm^{-1}$ and in the range of 1500–1600 $cm^{-1}$, the characteristic band of ordered graphite is observed [42].

In Fig. 6, the spectra of the used samples are shown together with the images obtained through the confocal microscope. The Raman spectra of the post-reaction samples did not show significant differences in the carbon species formed, with characteristic graphitic carbon bands at 1325 $cm^{-1}$ (C $sp^3$) and 1600 $cm^{-1}$ (C $sp^2$) for all Ni contents. In the post-reaction RhNiHT25 catalyst, no characteristic signals of carbon were detected, which confirms that Rh blocks carbon deposition.

The SEM analyses of the NiHT1 post-reaction sample allowed us to confirm the presence of a high amount of carbonaceous filaments, whisker-like in NiHT1 (Fig. 7). The carbon deposition does not affect the catalyst performance and its morphology could explain the low deactivation in spite of the high carbon content observed, mainly for NiHT1, where the Ni particle is carried out to the filament tip.

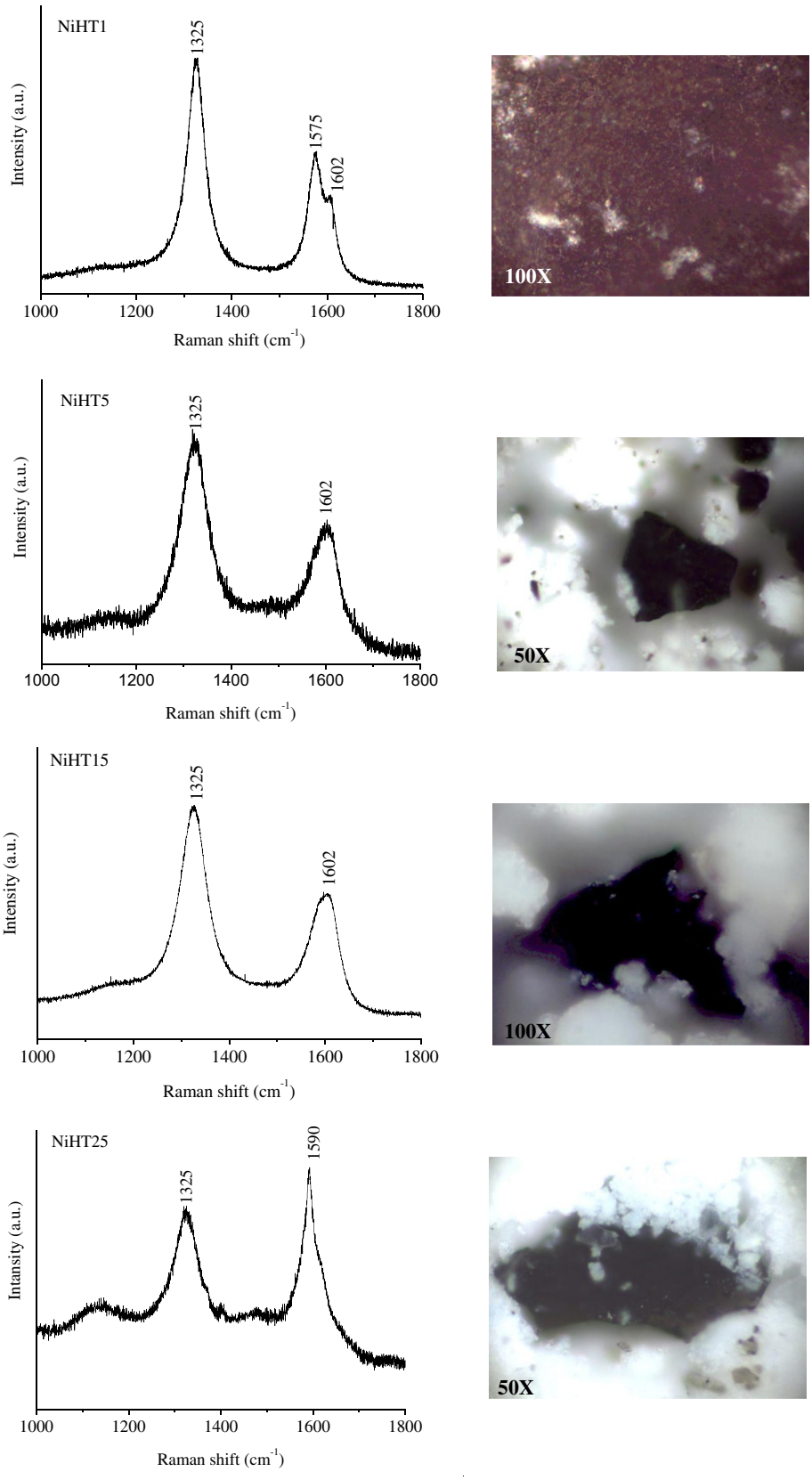


**Fig. 6 – Raman spectra and images obtained through the confocal microscope of the post-reaction samples.**

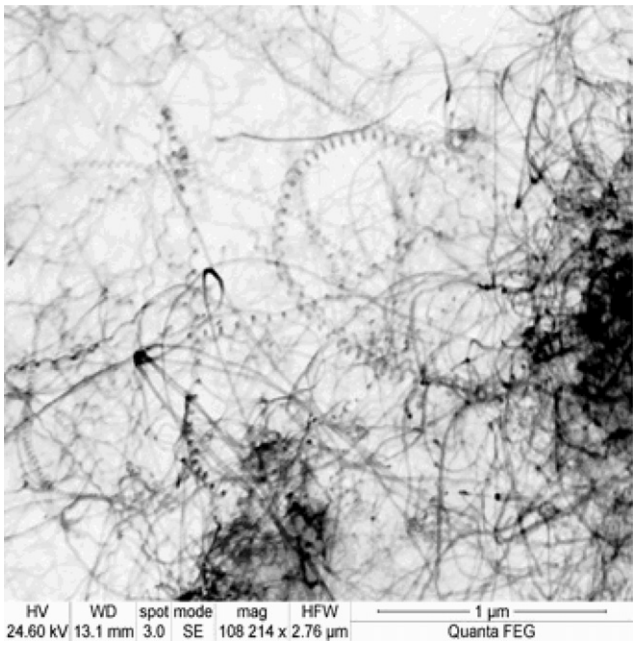


**Fig. 7 – SEM micrograph of the NiHT1 post-reaction sample.**

## 4. Conclusions

NiHTx catalysts with high Ni content (x = 1 and 5) showed high stability and high methane conversion for the partial oxidation of methane at 750 °C. On the other hand those with lower Ni content (x = 15 and 25) exhibited low catalytic activity with low $H_2$/CO ratio (<2) and fast deactivation.

At 550 °C, the water gas shift reaction was favored, increasing the hydrogen yield. However, the occurrence of the Boudouard reaction produced high carbon deposition with the formation of whisker-type carbon.

In the bimetallic RhNiHT25, the Ni reducibility was improved due to the synergic effect between Rh and Ni, increasing the methane conversion and hydrogen selectivity. In addition, the noticeable increase in stability was related to the absence of carbon deposition after 30 h on stream (at 750 and 550 °C).

These results show that the bimetallic catalyst is promising for application in membrane reactors to produce high purity hydrogen. However, additional studies are necessary to optimize the Rh content in the bimetallic NiHT catalyst.

## Acknowledgements

We thank the International Cooperation Project CONICET (Argentina)/CNPq (Brazil) Res 473/11 and 457/12 for the financial support.

REFERENCES

[1] IEA. http://www.iea.org.
[2] Rostrup-Nielsen T. Manufacture of hydrogen. Catalysis Today 2005;106:293.
[3] Enger C, Lodeng R, Holmen A. A review of catalytic partial oxidation of methane to synthesis gas with emphasis on reaction mechanisms over transition metal catalysts. Applied Catalysis A 2008;346:1–27.
[4] Chen Y, Zhou W, Shao Z, Xu N. Nickel catalyst prepared via glycine nitrate process for partial oxidation of methane to syngas. Catalysis Communications 2008;9:1418–25.
[5] Beretta A, Donazzi A, Groppi G, Forzatti P, Dal Santo V, Sordelli L, et al. Testing in annular micro-reactor and characterization of supported Rh nanoparticles for the catalytic partial oxidation of methane: effect of the preparation procedure. Applied Catalysis B Environmental 2008;83:96–109.
[6] Song Y, Liu H, Liu S, He D. Partial oxidation of methane to syngas over Ni/$Al_2O_3$ catalysts prepared by a modified sol–gel method. Energy & Fuels 2009;23:1925–30.
[7] Kim W, Kan M, Kwak Y. Preparation of supported Ni catalysts with a core/shell structure and their catalytic tests of partial oxidation of methane. International Journal of Hydrogen Energy 2009;34:3351–9.
[8] Basile F, Vaccari A. Application of hydrotalcite-type anionic clays (layered double hydroxides) in catalysis. In: Rives V, editor. Layered double hydroxides: present and future. New York: Nova Science; 2001. p. 285–321.
[9] Basile F, Fornasari G, Vaccari A. Catalytic activity of layered double hydroxides or hydrotalcite-type anionic clays. In: Hubbard E, editor. Encyclopedia of surface and colloid science. New York: Deker; 2002. p. 909–30.
[10] Tichit D, Gerardin C, Durand R, Coq B. Layered double hydroxides: precursors for multifunctional catalysts. Topics in Catalysis 2006;39:89–96.
[11] Christensen K, Lødeng C, Holmen A. Effect of supports and Ni crystal size on carbon formation and sintering during steam methane reforming. Applied Catalysis A 2006;314:9–22.
[12] Bhattacharyya A, Chang V, Schumacher D. $CO_2$ reforming of methane to syngas I: evaluation of hydrotalcite clay-derived catalysts. Applied Clay Science 1998;13:317–28.
[13] Takehira K, Shishido T, Wang P, Kosaka T, Takaki K. Autothermal reforming of $CH_4$ over supported Ni catalysts prepared from Mg–Al hydrotalcite-like anionic clay. Journal of Catalysis 2004;221:43–54.
[14] Shishid T, Sukenobu M, Morioka H, Kondo M, Wang Y, Takaki K, et al. Partial oxidation of methane over Ni/Mg–Al oxide catalysts prepared by solid phase crystallization method from Mg–Al hydrotalcite-like precursors. Applied Catalysis A 2002;223:35–42.
[15] Basile F, Fornasari G, Gazzano M, Vaccari A. Rh, Ru and Ir catalysts obtained by HT precursors: effect of the thermal evolution and composition on the material structure and use. Journal of Material Chemistry 2002;12:3296–303.
[16] Basile F, Fornasari G, Rosetti V, Trifirò F, Vaccari A. Effect of the Mg/Al ratio of the hydrotalcite-type precursor on the dispersion and activity of Rh and Ru catalysts for the partial oxidation of methane. Catalysis Today 2004;91-92:293–7.
[17] Jun Z, Ning Z, Wei W, Yuhan S. Partial oxidation of methane over Ni/Mg/Al/La mixed oxides. Prepared from layered double hydrotalcites. International Journal of Hydrogen Energy 2010;35:11,776–11,786.
[18] Lucredio A, Assaf J, Assaf E. Applied Catalysis A: General 2011;400:156–65.
[19] Rietveld H. A profile refinement method for nuclear and magnetic structures. Journal of Applied Crystallography 1969;2:65–71.
[20] Froment GF, Bischoff KB. Chemical reactor analysis and design. New York: Wiley; 1979.
[21] Cavani F, Trifiro F, Vaccari A. Hydrotalcite-type anionic clays: preparation, properties and applications. Catalysis Today 1991;11:173–301.

[22] Lebedeva O, Tichit D, Coq B. Influence of the compensating anions of Ni/Al and Ni/Mg/Al layered double hydroxides on their activation under oxidising and reducing atmospheres. Applied Catalysis A: General 1999;183:61–7.
[23] Tichit D, Medina F, Coq B, Dutarte R. Activation under oxidizing and reducing atmospheres of Ni-containing layered double hydroxides. Applied Catalysis A: General 1997;159:241–58.
[24] Rey F, Fornés V, Rojo J. Thermal decomposition of hydrotalcites. An infrared and nuclear magnetic resonance spectroscopic study. Journal of Chemical Society Faraday Transactions 1992;88:2233–8.
[25] Camacho Rodrigues S, Assumpção Henriques C, Fontes Monteiro J. Influence of Ni content on physico-chemical characteristics of Ni, Mg, Al-Hydrotalcite like compounds. Materials Research 2003;6:563–8.
[26] Daza C, Gallego J, Moreno J, Mondragón F, Moreno S, Molina R. $CO_2$ reforming of methane over Ni/Mg/Al/Ce mixed oxides. Catalysis Today 2008;133-135:357–66.
[27] Jirátová P, Cuba F, Kovanda L, Pitchon H. Preparation and characterisation of activated Ni(Mn)/Mg/Al hydrotalcites for combustion catalysis. Catalysis Today 2002;76:43–53.
[28] Tsyganok A, Tsunoda T, Hamakawa S, Suzuki K, Takehira K, Hayakawa T. Dry reforming of methane over catalysts derived from nickel-containing Mg–Al layered double hydroxides. Journal of Catalysis 2003;213:191–203.
[29] Chmielarz L, Kustrowski P, Lasocha A, Dziembaj R. Influence of Cu, Co and Ni cations incorporated in brucite-type layers on thermal behaviour of hydrotalcites and reducibility of the derived mixed oxide systems. Thermochimica Acta 2003;395:225–36.
[30] Basile F, Basini L, D'Amore M, Fornasari G, Guarinoni A, Matteuzzi D, et al. Ni/Mg/Al anionic clay derived catalysts for the catalytic partial oxidation of methane: residence time dependence of the reactivity features. Journal of Catalysis 1998;173:247–56.
[31] Nefedov I, Firsov N, Shaplygin S. Electronic structures of $MRhO_2$, $MRh_2O4$, $RhMO_4$ and $Rh_2MO_6$ on the basis of X-ray spectroscopy and ESCA data. Journal of Electron Spectroscopy and Related Phenomena 1982;26:65.
[32] Gysling H, Monnier R, Apai G. Synthesis, characterization, and catalytic activity of $LaRhO_3$. Journal of Catalysis 1987;103:407.
[33] Polychronopoulou K, Fierro J, Efstathiou AM. The phenol steam reforming reaction over MgO-based supported Rh catalysts. Journal of Catalysis 2004;228:417.
[34] Romero A, Jobbagy M, Laborde M, Baronetti G, Amadeo N. Ni(II)–Mg(II)–Al(III) catalysts for hydrogen production from ethanol steam reforming: Influence of the activation treatments. Catalysis Today 2010;149:407–12.
[35] Ferrandon M, Kropf A, Krause T. Bimetallic Ni-Rh catalysts with low amounts of Rh for the steam and autothermal reforming of n-butane for fuel cell applications. Applied Catalysis A 2010;379:121–8.
[36] Medina F, Tichit D, Coq B, Vaccari A, Dung N. Hydrogenation of acetonitrile on nickel-based catalysts prepared from hydrotalcite-like precursors. Journal of Catalysis 1997;167:142–52.
[37] Melo F, Morlanes N. Synthesis, characterization and catalytic behaviour of NiMgAl mixed oxides as catalysts for hydrogen production by naphtha steam reforming. Catalysis Today 2008;133-135:383–93.
[38] Basile F, Basini L, Fornasari G, Guarinoni A, Trifiro F, Vaccari A. Catalytic behaviour of Ni- and Rh-containing catalysts in the partial oxidation of methane at short residence times. Studies in Surface Science and Catalysis 1998;119:693.
[39] Basile F, Fornasari G, Trifirò F, Vaccari A. Rh–Ni synergy in the catalytic partial oxidation of methane: surface phenomena and catalyst stability. Catalysis Today 2002;77:215–23.
[40] Narksitipan S, Thongtem T, Thongtem S. Characterization of $sp^3$ carbon produced by plasma deposition on gamma-TiAl alloys. Applied Surface Science 2008;254:7759–64.
[41] Arepalli S, Nikolaev P, Gorelik O, Hadjiev V, Holmes W, Files B, et al. Protocol for the characterization of single-wall carbon nanotube material quality. Carbon 2004;42:1783–91.
[42] Berlin T, Epron F. Characterization methods of carbon nanotubes: a review. Materials Science and Engineering: B 2005;119:105–18.